Journal of Materials Science: Materials in Electronics (2020) 31:10355–10365
https://doi.org/10.1007/s10854-020-03583-5

Effect of V doping on electrical and magnetic properties of $La_{0.71}Ca_{0.29}MnO_3$ polycrystalline ceramics

Ping Yu[1] · Yule Li[1] · Fuxin Ling[1] · Longfei Qi[1] · Ling Li[1] · Qingming Chen[1] · Hui Zhang[1]

Received: 21 February 2020 / Accepted: 11 May 2020 / Published online: 28 May 2020

Abstract
A series of $La_{0.71}Ca_{0.29}Mn_{1-x}V_xO_3$ ($x = 0.00, 0.01, 0.03, 0.05, 0.10$) ceramic samples were synthesized via sol–gel method. Structural, electric, and magnetic transport properties of samples were characterized. Results show that all samples have perovskite phases, and no impurity phases were detected. Slight doping with V on B sites does not change perovskite structure of samples, but the doping leads to lattice distortion through modifying Mn–O bond lengths and Mn–O–Mn bond angles. The cell volume increased, melting point decreased, and abnormal grain growth occurred as the content of V increased. Temperature dependence of sample resistivities (ρ–T) was tested using standard four-probe method. Results show that slight doping with V can effectively increase temperature coefficient of resistance (TCR) up to 37.04% K^{-1} ($x = 0.01$). However, this decreases metal–insulator transition temperature (T_{MI}). Meanwhile, ρ–T dependence in magnetic field (1 T) shows that V substituting for Mn can significantly increase magnetoresistance of $La_{0.71}Ca_{0.29}MnO_3$ near room temperature by ~ 78.3%, showing the promise of this material for use in magnetoresistive sensors, contactless magnetoresistive switches, and memories.

1 Introduction

Perovskite manganite materials are strongly correlated electronic materials. With the discovery of colossal magnetoresistance (CMR), these materials have important research value and many potential applications, and they are one of the most advanced research topics in condensed matter physics and material science in recent decades [1–3]. Perovskite manganite materials have attracted much attention in information storage and magnetic sensitive elements, it has the same general structural formula $RE_{1-x}A_xMnO_3$, where RE represents positive trivalent rare earth ions (e.g., La^{3+}, Sm^{3+}, or Nd^{3+}). A is a positive divalent alkali metal ion (e.g., Sr^{2+} or Ca^{2+}) [4, 5].

In 1993, Helmolt et al. observed magnetoresistance effects up to several orders of magnitude in La–Ba–Mn–O thin films [6], and Zener explained their origin using the double exchange model. Nowadays, double exchange is considered one of the reasons giving rise to the ferromagnetic properties and metallic behavior of these materials [7, 8]. It is generally believed that the interaction between the intrinsic double exchange mechanism and Jahn–Teller distortion causes a metal–insulator phase transition. So far, magnetoresistance in perovskite manganese oxide structure is the most significant. As an example, $La_{1-x}Ca_xMnO_3$ (ABO_3 type) [9] has a relatively clear electronic phase diagram. $La_{1-x}Ca_xMnO_3$ materials have great application prospects in magnetoresistance sensors, contactless magnetoresistance switches, and room temperature magnetic refrigeration materials; thanks to their metal–insulator transition properties. The electrical properties of these systems are generally measured using two parameters: temperature coefficient of resistance (TCR) and metal–insulator transition temperature (T_{MI}) [10–12]. We hope to achieve a high TCR with a T_{MI} value near room temperature, which can broaden the application range of this class of materials.

Magnetoresistance is widely used in sensors and memories. It was first discovered by William Thomson in 1857 in ferromagnetic polycrystals. Related effects include colossal magnetoresistance, tunnel magnetoresistance, and ballistic magnetoresistance. MR is defined as: $MR = [R(0) - R(H)]/R(H) \times 100\%$, where $R(0)$ and $R(H)$ are the resistance values in the absence of a magnetic field and in an applied magnetic field, respectively. The magnitude of a material's MR value reflects its sensitivity to an external magnetic field.

✉ Hui Zhang
harry_zhang71@163.com

[1] Faculty of Materials Science and Engineering, Kunming University of Science and Technology, Kunming 650093, People's Republic of China

Results from many studies show that the electromagnetic properties of $La_{1-x}Ca_xMnO_3$ can be studied by changing the doping of A and B sites[13–15]. In $La_{1-x}Ca_xMnO_3$, double exchange between Mn^{3+} and Mn^{4+} affects the resistivity, TCR, and T_{MI} of the material [16, 17]. Commonly used substitute ions for B-site doping include Ni, Cr, Fe, Co, and V. The average radius, charge, ionic polarization, tolerance factor, oxygen deficiency, and ion mismatch of B-site cations all affect the giant magnetoresistance effect observed from the $La_{1-x}Ca_xMnO_3$ material. The primary factors influencing giant magnetoresistance are ionic polarization, average radius, and the ability of transition metal ions to form a perovskite structure [18–21]. In contrast to doping A-sites with metal ions, B sites doped with metal ions do not directly participate in the double exchange action, rather changing the ratio of Mn^{3+} to Mn^{4+}. This influences the double exchange action through magnetic coupling with Mn and affects the electrical and magnetic properties of the material [22–24].

At present, much research has focused on incorporation of different ions into perovskite manganese oxides at the A-site. However, the incorporation of different metal ions in the B-site was not examined in previous studies and deserves further investigation, so we choose V as doping ion for this study. The TCR of $La_{0.71}Ca_{0.29}MnO_3$ as parent compound is higher than $La_{0.67}Ca_{0.33}MnO_3$ as parent compound [2, 25]. In this paper, $La_{0.71}Ca_{0.29}MnO_3$ with perovskite structure was used as a parent compound to prepare a series of samples containing V instead of Mn, in order to increase the TCR and MR values. Studying the effects of V doping on the magnetic and electrical transport properties of $La_{0.71}Ca_{0.29}Mn_{1-x}V_xO_3$ ceramics in this study, and to maximize the TCR and MR values by adjusting the V doping content.

2 Experiments

$La_{0.71}Ca_{0.29}Mn_{1-x}V_xO_3$ ($x = 0.00$, 0.01, 0.03, 0.05, 0.10) ceramics were prepared by a sol–gel method using NH_4VO_3 as the doping source and methanol as the solvent. According to the stoichiometric ratio, high-purity $La(NO_3)_3{\cdot}xH_2O$, $Ca(NO_3){\cdot}24H_2O$, $Mn(NO_3){\cdot}24H_2O$, NH_4VO_3 and $C_6H_8O_7{\cdot}H_2O$ as a chelating agent were weighed and mixed in a beaker. The molar ratio of metal ions and citric acid was 1:4. The beaker was stirred continuously with a magnetic stirrer. After the precipitate was completely dissolved, 5 mL of ethylene glycol was added as a dispersant, and stirring continued for 20 min. Then, the mixture was placed in a thermostatic magnetic water bath for 25 min at 88 °C. After the solution formed a wet gel, it was quickly removed from the bath and placed in a 140 °C air drying oven. A dry gel was produced after drying for 24 h. Next, the xerogel was placed in an agate mortar and ground for 30 min to obtain a powder. The sample powder was placed in a crucible and calcined for 13 h in a box furnace at 500 °C. The calcined sample was taken out, and 2 g of the material was weighed and pressed into a pellet-shaped target with 20 mm diameter. The target was sintered at 1400 °C in air atmosphere for 22 h to obtain a series of $La_{0.71}Ca_{0.29}Mn_{1-x}V_xO_3$ ($x = 0.00$, 0.01, 0.03, 0.05, 0.10) samples.

The elemental distribution of the polycrystalline ceramics was determined with EDS to determine the phase content in the grains and grain boundaries of the polycrystalline ceramics. The crystal structure of the polycrystalline ceramic was characterized using X-ray diffraction (XRD) with CuK_α radiation (0.154056 nm) at room temperature. The microstructure and surface morphology of the ceramic samples were examined with a scanning electron microscope (SEM, Hitachi SU8010). The resistance temperature curves of all samples were measured using a standard four-probe method at temperatures ranging from 150 to 300 K. The magnetization temperature curve of the ceramic sample was measured with a superconducting quantum interference device (SQUID-VSM) magnetic measurement system in a 100 Oe magnetic field at temperatures ranging from 100 to 300 K.

3 Results and discussion

3.1 Valence element analysis with XPS

Figure 1a shows an XPS spectrum from the $La_{0.71}Ca_{0.29}Mn_{1-x}V_xO_3$ ($x = 0.00$, 0.01, 0.03, 0.05, 0.10) polycrystalline ceramics, which confirms La, Ca, Mn, O, and V were present on the surface of the polycrystalline target. Figure 1b shows a fit of the characteristic peak to the V-2p satellite peak. The test results show that the position of the characteristic V peak (517 eV) is consistent with the characteristic peak of V^{5+}, thus the valence state of V in $La_{0.71}Ca_{0.29}Mn_{1-x}V_xO_3$ is +5.

We carefully performed fitting for the XPS data of $La_{0.71}Ca_{0.29}Mn_{0.85}V_{0.15}O_3$, as seen in Fig. 1c. Shirley type background was selected, thereafter the standard Gaussian fitting for Mn-2p core level spectra was performed. The fitting result showed that the ratio of Mn^{3+} and Mn^{4+} was 3.90 through calculating the peak area, where the binding energies 641.2 eV for Mn^{3+}-$2p_{3/2}$ and 643.7 eV for Mn^{4+}-$2p_{3/2}$ were used. (The detailed parameters and results are summarized in Table 1.) For the first sight, this result conflicted

Table 1 Fitting results of Mn-$2p_{3/2}$ core level spectrum for $La_{0.71}Ca_{0.29}Mn_{0.85}V_{0.15}O_3$

Species	Position (eV)	Peak area	FWHM (eV)	Amount
Mn^{3+}	641.2	48024.3	3.05	0.68
Mn^{4+}	643.7	12328.0	3.09	0.17

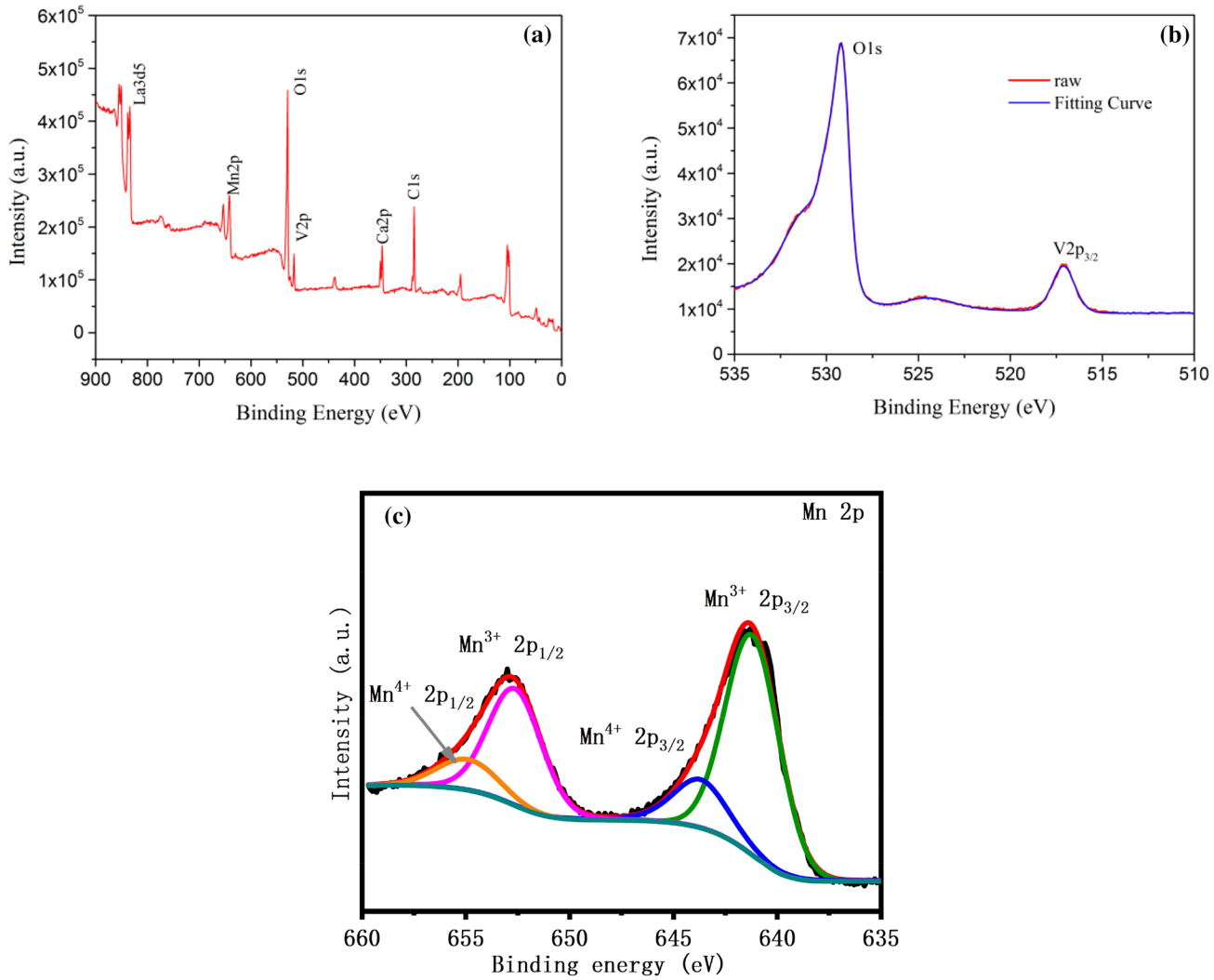

Fig. 1 **a** XPS full spectrum of $La_{0.71}Ca_{0.29}Mn_{0.85}V_{0.15}O_3$ sample, **b** V-2p peak fitting full spectrum. **c** Fitting of Mn-2p core level spectra of $La_{0.71}Ca_{0.29}Mn_{0.85}V_{0.15}O_3$. Mn-2p core level spectra. Red solid line: the fitting result; blue solid line: Mn^{4+}-$2p_{3/2}$; green solid line: Mn^{3+}-$2p_{1/2}$ (Color figure online)

with simple estimation of Mn^{3+} and Mn^{4+} amount from the formula $La_{0.71}Ca_{0.29}Mn_{0.85}V_{0.15}O_3$, which suggested the amount of Mn^{4+} approached 0. However, taken into account of volatility of La, Ca, especially V, we thought this result was acceptable. (V exhibited 5^+ in $La_{0.71}Ca_{0.29}Mn_{0.85}V_{0.15}O_3$ as seen in the paper, the melting point of V_2O_5 is only around 700 °C. Further, one had to decrease the sinter temperature for $La_{0.71}Ca_{0.29}MnO_3$ with V doping owing to the same reason.)

3.2 Analysis of the XRD patterns

Figure 2a shows XRD diffraction patterns from the polycrystalline ceramics. All samples are typical pure phase perovskite structures, and no other phases were detected. All diffraction peaks from all samples are sharp, indicating the ceramic samples are crystalline. In addition, one can see that doping with V causes preferential growth along the (321) direction, which is related to the lower melting point of V_2O_5. Figure 2b shows a magnified view of the (121) peaks. The strongest diffraction peak moves toward smaller angles as the content of V increases. This means the volume of the unit cell increased.

Because the effective ionic radius of V^{5+} is 0.54 Å, the ionic radii of Mn^{3+}, Mn^{4+}, La^{3+}, and Ca^{2+} are 0.645, 0.53, 1.22, and 1.18 Å, respectively. V^{5+} will replace some Mn^{4+} to cause an increase in the unit cell volume. However, the radius difference between V^{5+} and Mn^{4+} is trivial. A more likely reason is the increase of Mn^{3+} content by V doping due to charge neutrality, which leads to the unit cell volume increase, thus shifting the (121) diffraction peak to a smaller angle.

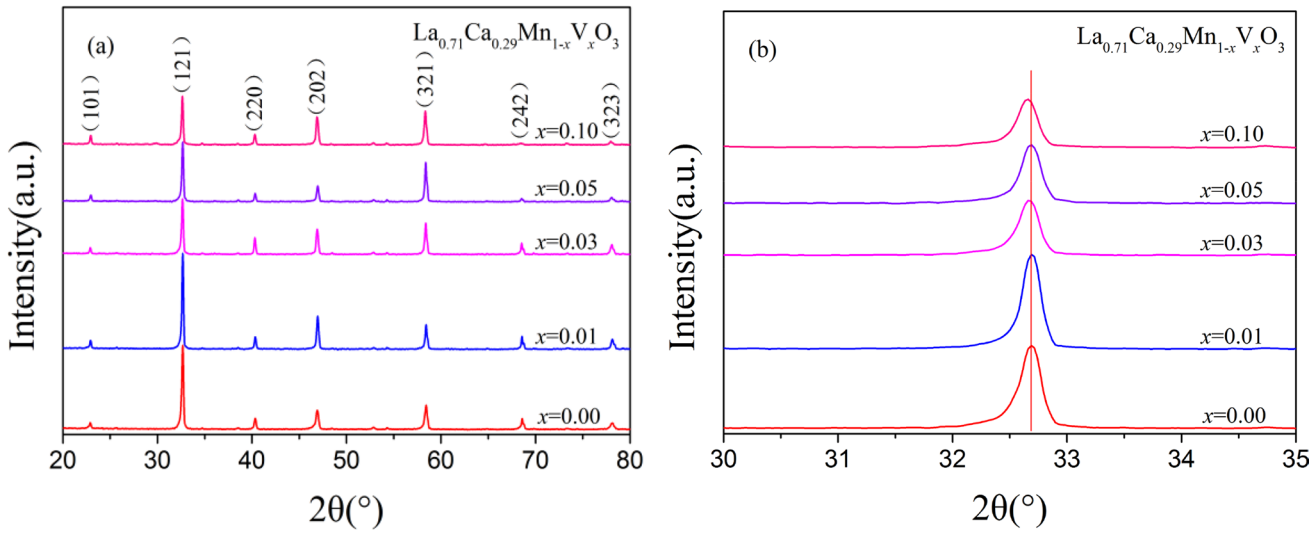

Fig. 2 **a** $La_{0.71}Ca_{0.29}Mn_{1-x}V_xO_3$ XRD diffraction pattern, **b** magnified view of the strongest diffraction peak

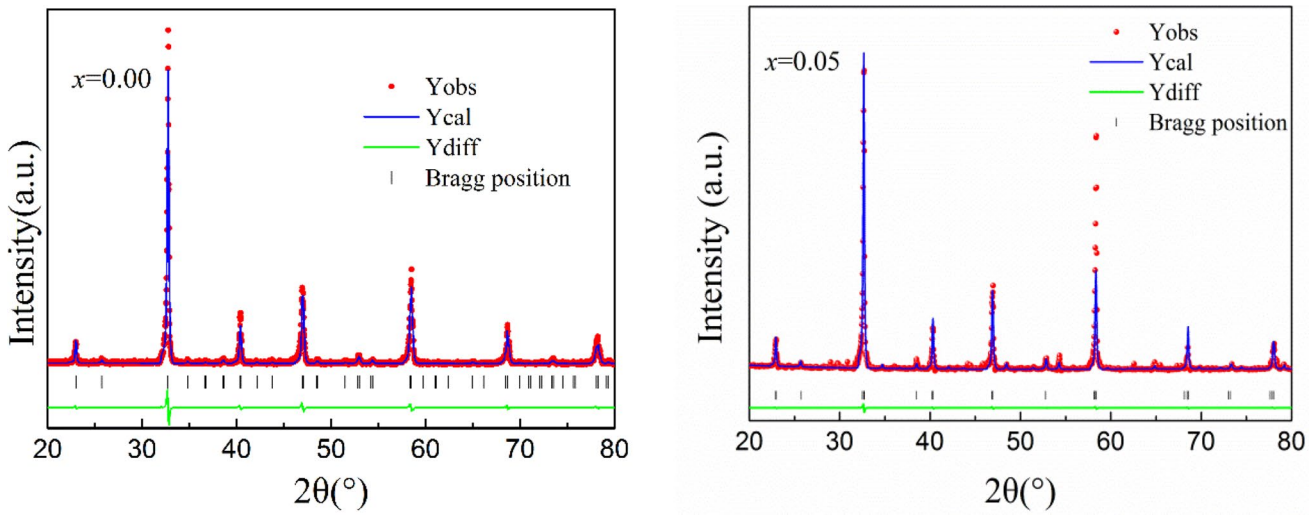

Fig. 3 Refined fitting curve with $x = 0.00$ and $x = 0.05$ (Color figure online)

Figure 3 shows Rietveld XRD patterns from the samples with $x = 0.00$ and $x = 0.03$. The red dot represents diffraction data, the blue line shows the fitting results, the short vertical line shows a fit to the diffraction peak position, and the green line shows the difference between the measured and the fitted values. One can see that the sample is crystalline with no second phases or impurities.

Table 2 shows Rietveld refinement results. One can see that the crystal structure of all samples is orthorhombic. The goodness of the fit (χ) values was near 1, indicating the suitability of the fitting model. The agreement factors (R_p, R_b, and R_e) are within a reasonable range ($R_p < 10\%$, $R_b < 15\%$, and $R_e < 10\%$, respectively). The cell volume increased as x increased, which produces changes in the Mn–O bond distance and Mn–O–Mn bond angles. Because the smaller proportion of V doping, it did not cause changes in the crystal structures.

3.3 The analysis of SEM micrographs

Figure 4a–d show the SEM images of $La_{0.71}Ca_{0.29}Mn_{1-x}V_xO_3$ ($x = 0.00$, 0.01, 0.03, 0.10) polycrystalline ceramics. Figure 4a has a magnification of 1000 times, and Fig. 4b–d has a magnification of 500 times, this is due to abnormal grain growth from V doping, and grains cannot be seen at

Table 2 Structural parameters and *R* values of the sample using Rietveld full spectrum fitting

x	0.00	0.01	0.03	0.05	0.10
Space group	*Pnma*	*Pnma*	*Pnma*	*Pnma*	*Pnma*
a (Å)	5.4599	5.4611	5.4633	5.4670	5.4693
b (Å)	7.7128	7.7194	7.7238	7.7262	7.7332
c (Å)	5.4801	5.4771	5.4800	5.4767	5.4840
Cell volume V (Å^3)	230.77	230.90	231.24	231.33	231.95
d_{Mn-O_1} (Å)	1.942	1.964	1.965	1.966	1.966
d_{Mn-O_2} (Å)	1.959	1.950	1.951	1.952	1.953
Mn–O_1–Mn (°)	161.298	158.549	158.550	158.569	158.561
Mn–O_2–Mn (°)	159.539	161.698	161.596	161.593	161.593
R_e (%)	5.7025	5.7500	7.4224	7.5893	7.5728
R_p (%)	4.2078	3.9175	5.2701	5.2465	6.5126
R_b (%)	5.6118	5.7671	7.4622	8.6563	9.5073
χ	0.97	1.01	1.01	1.30	1.57
τ	0.9301	0.9295	0.9283	0.9271	0.9240
$\langle r_{Mn} \rangle$ (Å)	0.61165	0.6129	0.6154	0.6179	0.6242

1000× magnification when $x = 0.01$, 0.03, 0.10. The average grain sizes in Fig. 4a–d are 17.4, 46.92, 111.98, and 138.34 μm, respectively. This indicates that V doping leads to growth of polycrystalline ceramic grains.

The SEM images show that the samples have clear grain boundaries (GBs) with few pores when the content of V is low. However, crystal grains in the samples grow abnormally as x increases, and precipitates appear at the GBs. When the content of V is high, the melting point of the samples will decrease, which will leads to overfiring (due to the low melting point of V_2O_5).

3.4 Element distribution analysis by EDS

Figure 5a, b shows an EDS surface scan spectrum from $La_{0.71}Ca_{0.29}Mn_{0.99}V_{0.01}O_3$ and $La_{0.71}Ca_{0.29}Mn_{0.9}V_{0.1}O_3$, respectively. Only a small portion of Mn is enriched, and

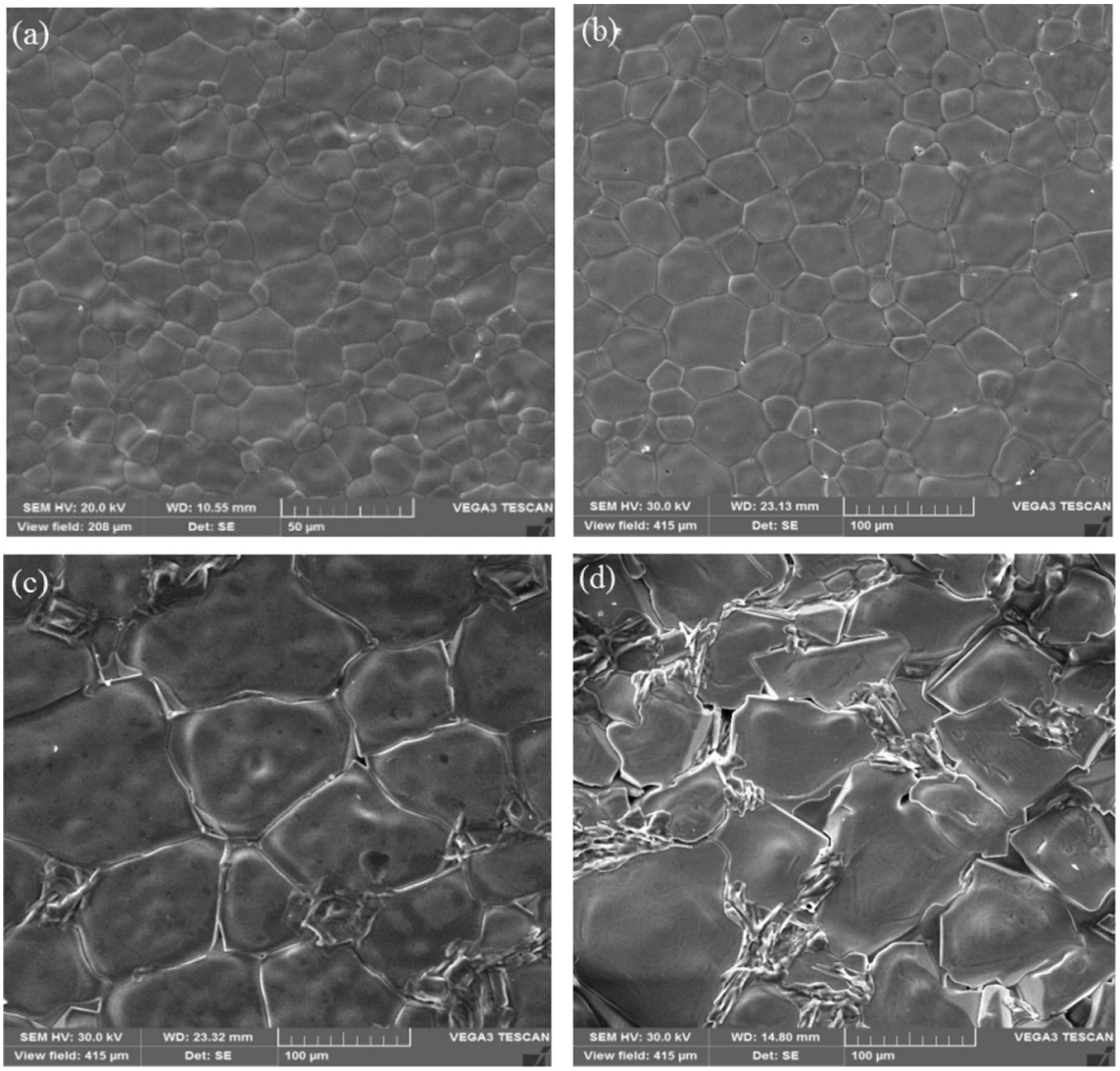

Fig. 4 SEM micrographs of $La_{0.71}Ca_{0.29}Mn_{1-x}V_xO_3$: **a** x = 0.00, 1000X;**b** x = 0.01, 500X; **c** = 0.03,500X; **d** x = 0.10,500X

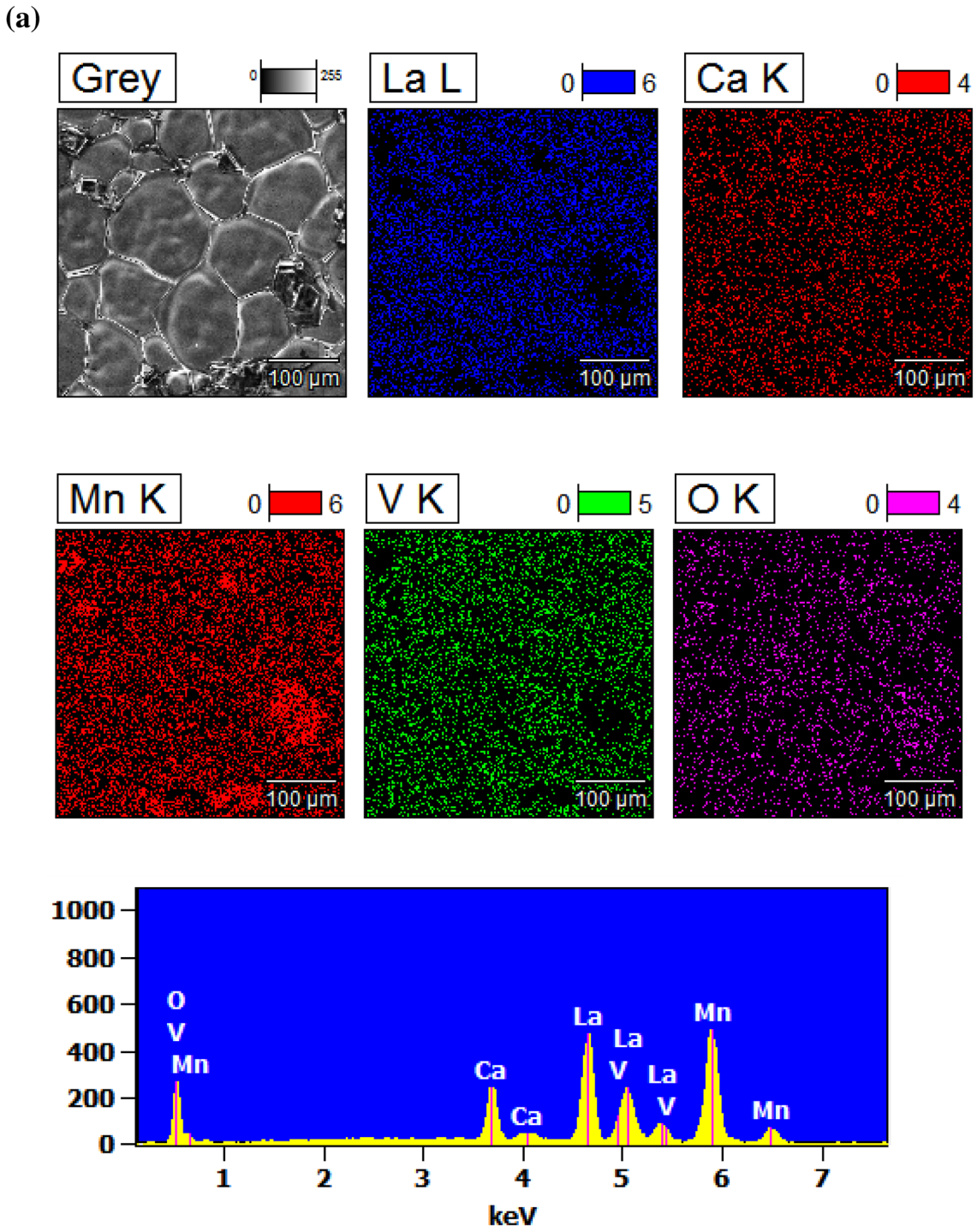

Fig. 5 **a** EDS surface sweep spectrum of $La_{0.71}Ca_{0.29}Mn_{0.99}V_{0.01}O_3$. **b** EDS surface sweep spectrum of $La_{0.71}Ca_{0.29}Mn_{0.9}V_{0.1}O_3$

all elements in the polycrystalline ceramic material are uniformly distributed. The enrichment of Mn is probably due to higher volatility of La, Ca, and V than Mn at elevated temperature. No other impurities or other phases were detected. This is confirmed by the XRD test results.

3.5 Electronic transport properties

Figure 6a shows the electric transport properties of $La_{0.71}Ca_{0.29}Mn_{1-x}V_xO_3$ composites ($x = 0.00$, 0.01, 0.03, 0.05, and 0.10) determined from resistance versus temperature measurements ranging from 100 to 300 K. All samples

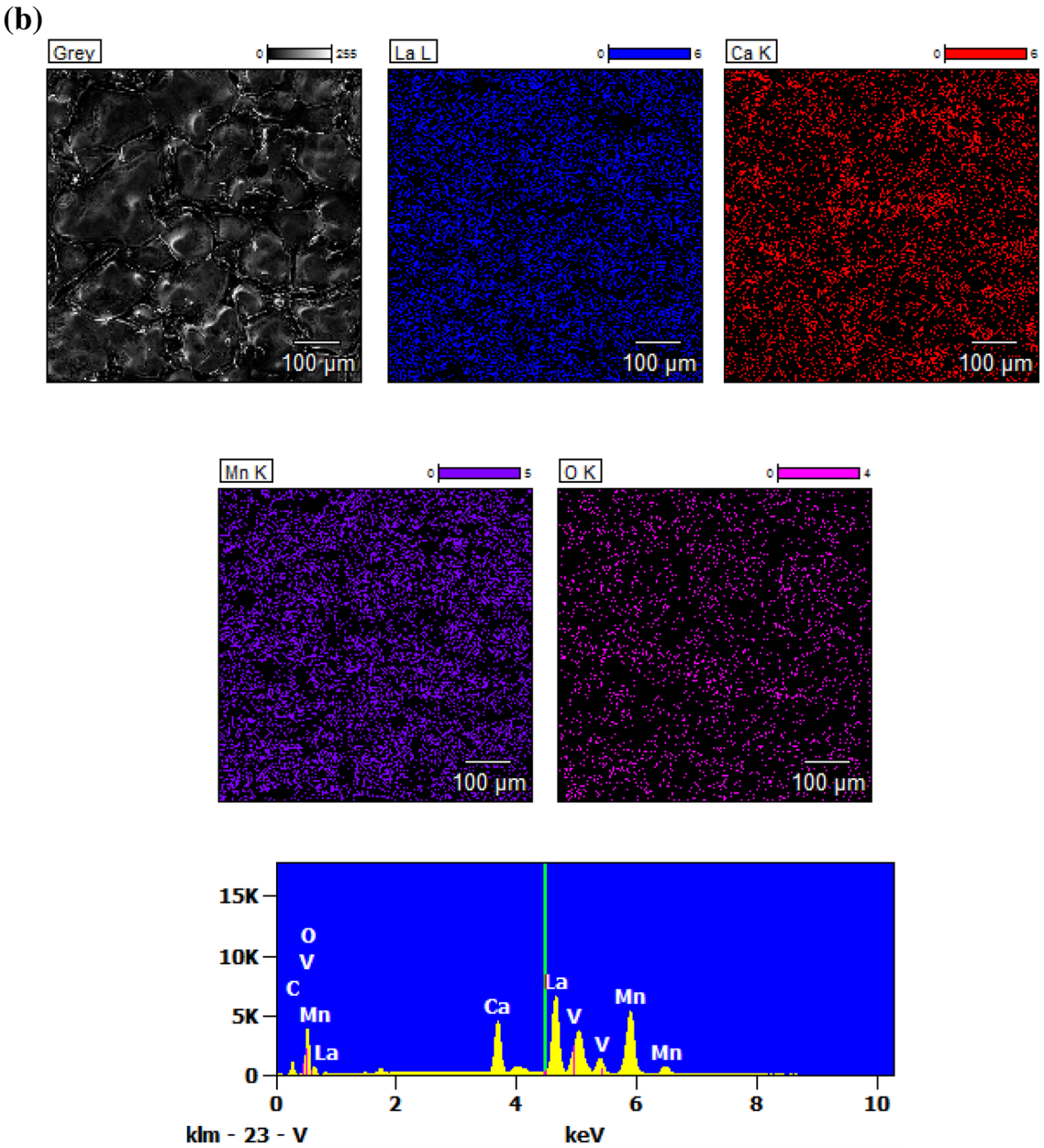

Fig. 5 (continued)

show a transition from low temperature ferromagnetic metallicity to high temperature insulation on both sides of T_{MI} as temperature increases, i.e., a metal insulator transition [20]. As V doping increased, the T_{MI} value of all samples moves toward the low temperature region, while the resistivity continuously increased. Results from previous studies show that the increased resistivity may be due to the weakening of double exchange. The resistance temperature curve of LaCaMnO:V_x ($x = 0.00$, 0.01, 0.03, and 0.05) shows multiple turns, which may be due to the presence of several different ferromagnetic phases in the samples and Mn vacancies caused by volatilization of V.

TCR curves of the $La_{0.71}Ca_{0.29}Mn_{1-x}V_xO_3$ ($x = 0.00$, 0.01, 0.03, 0.05, and 0.10) polycrystalline ceramic samples is shown in Fig. 6b. TCR is defined as:

$$\mathrm{TCR}(\%) = 1/\rho(\mathrm{d}\rho/\mathrm{d}T) \times 100\%,$$

where ρ and T are the resistance and temperature, respectively. According to the definition of TCR, the primary factors affecting the value of TCR are the resistivity ρ of the sample and the degree of temperature broadening at the

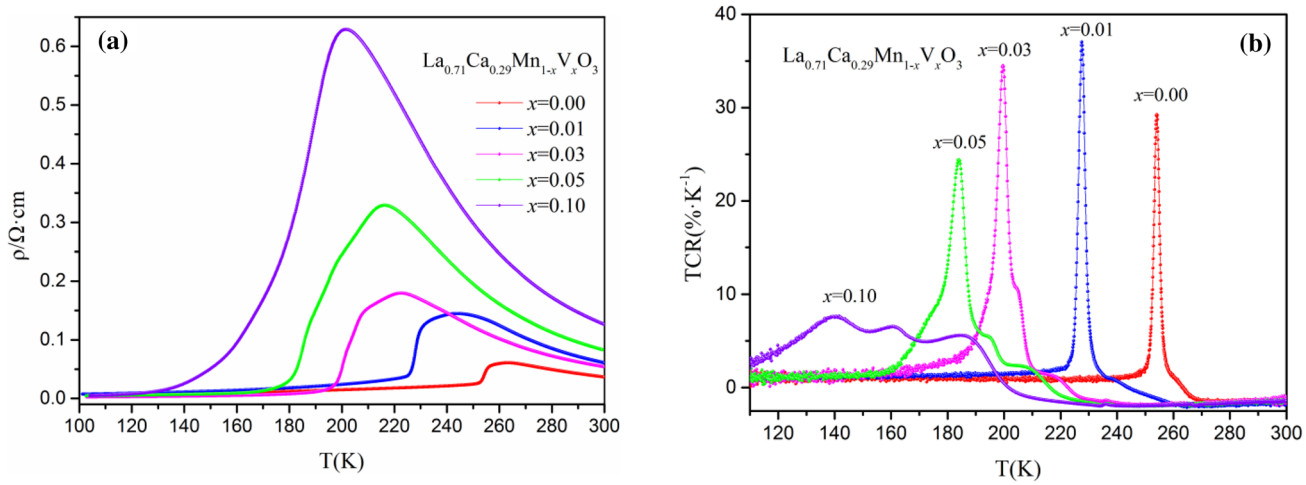

Fig. 6 **a** Resistivity versus temperature plots of $La_{0.71}Ca_{0.29}Mn_{1-x}V_xO_3$ ($x=0.00$, 0.01, 0.03, 0.05, 0.10) samples. **b** Variation in TCR (% K^{-1}) with temperature for $La_{0.71}Ca_{0.29}Mn_{1-x}V_xO_3$ composites

time of transition. Figure 6b and Table 3 show that the peak TCR first increased and then decreased as the content of V increased. At $x=0.01$, the maximum TCR (TCR_{max}) reached 37.04% K^{-1}, and T_{MI} moved toward the low temperature region. This is better than the results obtained in some literatures [19, 26]. The high TCR in the LCMVO:$V_{0.01}$ sample could allow this material to be used in a bolometer. The effect of increasing V on TCR can be explained as follows: Because the effective ionic radius of V^{5+} is 0.54 Å, the ionic radii of Mn^{3+}, Mn^{4+} are 0.645, 0.53 Å, respectively. With the increase of V doping, Mn^{3+} will increase. The radius difference between V^{5+} and Mn^{3+} is large, with the doping of V, the double exchange of Mn^{3+}–O–Mn^{4+} is blocked to keep the charge balance, thus the T_{MI} decreased and the resistivity increased. TCR is affected by many factors, among which grain size is one of the main factors [27]. It can be known from Table 3 that the TCR of the 0.01-doped sample has significantly increased compared to the undoped sample. SEM image results show that the grain size increases significantly when the V doping content exceeds 0.01, which may be the main reason for the increase in TCR. At the same time, we can see that with the increase of V doping, the grain size is still increasing, but TCR is not increasing. The reason is that the grain size of the samples doped with 0.03 and 0.1 is large, but the density is obviously decreased, the porosity and defects in the samples are increased, so the TCR is not increased.

Table 3 The metal–insulator transition temperature Tp, the temperature coefficient of resistivity (TCR), and the resistivity for the $La_{0.71}Ca_{0.29}Mn_{1-x}V_xO_3$ ($x=0.00$, 0.01, 0.03, 0.05) samples

Sample (x)	T_p (K)	TCR (% K^{-1})	ρ_{peak} (Ω cm)
$La_{0.71}Ca_{0.29}MnO_3$	262.6	29.24	0.06091
$La_{0.71}Ca_{0.29}Mn_{0.99}V_{0.01}O_3$	243.5	37.04	0.14503
$La_{0.71}Ca_{0.29}Mn_{0.97}V_{0.03}O_3$	222.7	34.49	0.17987
$La_{0.71}Ca_{0.29}Mn_{0.95}V_{0.05}O_3$	216.3	24.40	0.32910
$La_{0.71}Ca_{0.29}Mn_{0.9}V_{0.1}O_3$	201.6	7.67	0.62897

3.6 Magnetic characteristics

One can see from Fig. 7a–d that T_{MI} in the magnetic field is higher than that without a magnetic field. The resistivity of the samples also decreases. The reason for this phenomenon is that the local spin arrangement of electrons tends to be more ordered in a magnetic field, which is beneficial to hopping of e_g level electrons, thus increasing double exchange of Mn^{3+}–O–Mn^{4+}, which increases T_{MI} and decreases resistivity.

Figure 7e shows that increasing the content of V causes the peak MR value to first increase and then decrease, and the peak value moves to the low temperature region. This also shows that V doping can effectively increase the MR value of the samples from 190 to − 210 K. When $x=0.03$, MR can be as high as 78.30%, which is much higher than that without V [28]. As V occupies an Mn site, it directly blocks the double exchange of Mn^{3+}–O–Mn^{4+}, thereafter blocking the e_g electron conduction channel, i.e., the resistivity increases and T_{MI} decreases. However, unlike Cr, Fe, and Co, V^{5+} in oxygen octahedral seems capable of accepting an electron, thus T_{MI} decreases as the content of V increases, it is possibly related to the stronger covalency of the V–O bond and hybridization of V-3d and O-2p orbitals. In addition,

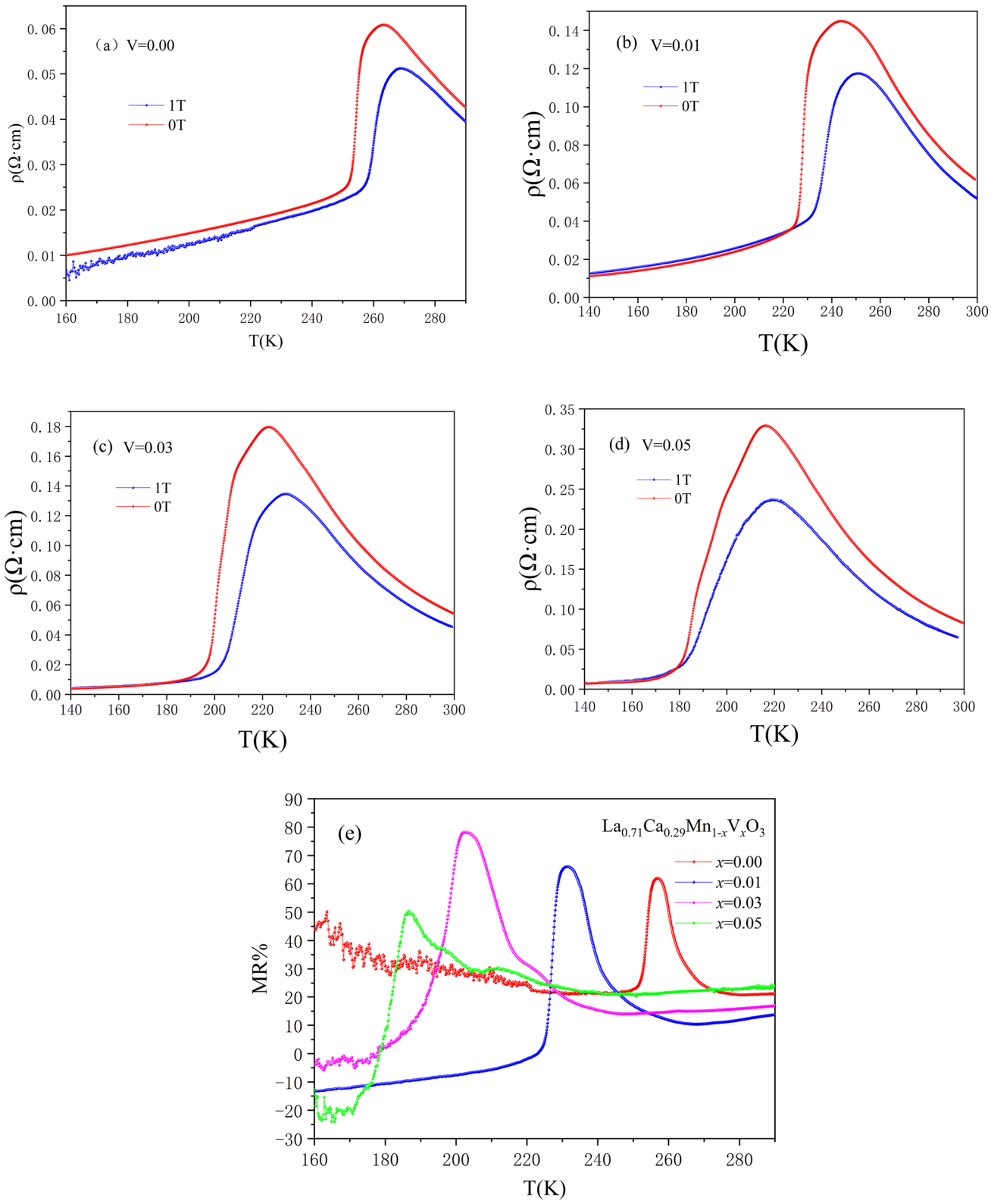

Fig. 7 **a**–**d** Magnetization of temperature for $La_{0.71}Ca_{0.29}Mn_{1-x}V_xO_3$ ($x=0.00$, 0.01, 0.03, 0.05) samples under an applied field of 100 Oe. **e** MR curve of $La_{0.71}Ca_{0.29}Mn_{1-x}V_xO_3$ ($x=0.00$, 0.01, 0.03, 0.05)

introduction of V into Mn sites will dilute Mn^{3+} and Mn^{4+}, which destroys the spin correlation between Mn^{3+} and Mn^{4+}, thus increasing the disorder of the spin orientation of Mn ions. However, the spin of Mn ions will align in an externally applied magnetic field, which increases double exchange and decreases resistivity near T_{MI}.

4 Conclusion

$La_{0.71}Ca_{0.29}Mn_{1-x}V_xO_3$ ($x = 0.00$, 0.01, 0.03, 0.05, 0.10) polycrystalline ceramic samples were prepared using a sol-gel method with an alcohol solvent. The effects of V doping on electrical and magnetic transport in the as-obtained samples were studied. XRD data and Rietveld show that all samples have a pure phase perovskite structure. Increasing the content of V increases the grain size and resistivity in LCMO:V_x, and the TMI value moved to a lower temperature and the TCR value first increased and then decreased. The TCR_{max} value for the sample with $x = 0.01$ was the largest, reaching 37.04% K^{-1}. At the optimal doping molar ratio of $x = 0.03$ in LCMO:V_x ceramics, the MR values reached up to 78.30%. Combined with excellent electrical properties, these ceramics may become candidates for contactless reluctance switches and memories.

Acknowledgements This work was supported by the National Natural Science Foundation of China (No. 11564021).

References

1. A. Dhahri, M. Jemmali, E. Dhahri, E.K. Hlil, Electrical transport and giant magnetoresistance in $La_{0.75}Sr_{0.25}Mn_{1-x}Cr_xO_3$ (0.15, 0.20 and 0.25) manganite oxide. Dalton Trans. **44**, 5620–5627 (2015)
2. X.X. Zhang, R.H. Yu, J. Tejada, G.F. Sun, Y. Xin, K.W. Wong, Magnetic properties and giantmagnetoresistance in $La_{0.67}Ca_{0.33}MnO_x$ bulk material. Appl. Phys. Lett. **68**, 3191–3193 (1996)
3. K. Chahara, T. Ohno, M. Kasai, Y. Kozono, Magnetoresistance in magnetic manganese oxide with intrinsic antiferromagnetic spin structure. Appl. Phys. Lett. **63**, 1990–1992 (1993)
4. J.B. Goodenough, Electronic structure of CMR manganites (invited). J. Appl. Phys. **81**, 5330–5335 (1997)
5. G.V. Tendeloo, O.I. Lebedev, S. Amelinckx, Atomic and microstructure of CMR materials. J. Magn. Magn. Mater. **211**, 73–83 (2000)
6. Q. Huang, Z.W. Li, J. Li, C.K. Ong, Effect of Fe doping on high field magnetoresistance and low field magnetoresistance at zero field in polycrystalline $La_{0.7}Sr_{0.3}Mn_{1-x}Fe_xO_3$(x = 0–0.12) thin films. J. Appl. Phys. **89**, 7410–7412 (2001)
7. P.D. Gennes, Effects of double exchange in magnetic crystal. Phys. Rev. **118**, 141 (1960)
8. L.W. Lei, Z.Y. Fu, J.Y. Zhang, H. Wang, K. Niihara, Low field magnetoresistance of $La_{0.7}Ca_{0.3}MnO_3$ ceramics fabricated by fast sintering process. J. Alloys Compd. **530**, 164–168 (2012)
9. S. Mathur, H. Shen, Structural and physical properties of $La_{2/3}Ca_{1/3}MnO_3$ prepared via a modified sol-gel method. J. Sol-Gel Sci. Technol. **25**, 147–157 (2002)
10. F. Jin, H. Zhang, Q. Chen, Improved Curie temperature and temperature coefficient of resistance (TCR) in $La_{0.7}Ca_{0.3-x}Sr_xMnO_3$:$Ag_{0.2}$ composites. J. Alloys Compd. **747**, 1027–1032 (2018)
11. T. Sun, J. Jiang, Q. Chen, X. Liu, Improvement of room-temperature TCR and MR in polycrystalline $La_{0.67}$ ($Ca_{0.27}Sr_{0.06}$)MnO_3 ceramics by Ag 2.0 doping. Ceram. Int. **44**, 9865–9874 (2018)
12. R. Tripathi, V.P.S. Awana, H. Kishan, G.L. Bhalla, Search for room temperature high-TCR manganite/silver composites. J. Magn. Magn. Mater. **320**, 189–192 (2008)
13. Y. Kalyana Lakshmi, P.V. Reddy, Influence of silver doping on the electrical and magnetic behavior of $La_{0.7}Ca_{0.3}MnO_3$ manganites. Solid State Sci. **12**, 1731–1740 (2010)
14. X.L. Xu, Y. Li, F.F. Hou, Q. Cheng, R.Z. SU, Effect of Co substitution on magnetic ground state in $Sm_{0.5}Ca_{0.5}MnO_3$. J. Alloys Compd. **628**, 89–96 (2015)
15. S.P. Altintas, A. Amira, A. Varilci, C. Terzioglu, Influence of Gd-doping in $La_{0.7}Ca_{0.3}MnO_3$ on its structural and magneto-electrical properties. J Magn Magn Mater **324**, 1331–1336 (2012)
16. S.L. Yuan, Y.P. Yang, Z.C. Xia, G. Peng, G.H. Zhang, A substantial improvement in magnetoresistance by Cu doping at Mn sites of $La_{2/3}Ca_{1/3}MnO_3$. Solid State Commun. **123**, 55–58 (2002)
17. A.I. Shames, E. Rozenberg, M. Auslender, D. Mogilyansky, E. Sominski, A. Gedanken, Transition to electron doping in manganite system: Size-induced effects on magnetic order, probed by electron resonance technique. Solid State Commun. **151**, 1593–1598 (2011)
18. A. Krichene, P.S. Solanki, S. Rayaprol, V. Ganesan, W. Boujelben, D.G. Kuberkar, B-site bismuth doping effect on structural, magnetic and magnetotransport properties of $La_{0.5}Ca_{0.5}Mn_{1-x}Bi_xO_3$. Ceram. Int. **41**, 2637–2647 (2015)
19. G.W. Kim, S. Kumar, J. Chang, C.G. Lee, B.H. Koo, Magnetic and electrical properties of $La_{0.7}Ca_{0.3}Mn_{0.95}Co_{0.05}O_3$ epitaxial layers by pulsed laser deposition. Ceram. Int. **38**, 443–446 (2012)
20. L.M. Wang, C.Y. Wang, C.C. Tseng, Correlation of the temperature coefficient of resistivity for doped manganites to the transition temperature, polaron binding energy, and magnetic order. Appl. Phys. Lett. **100**, 232–403 (2012)
21. X. Chen, H. Zhang, F. Jin, X. Liu, Q. Chen, Fabrication of $La_{(x)}Nd_{0.67-x}Sr_{0.33}MnO_3$ polycrystalline ceramics by sol-gel method. J. Sol-Gel. Sci. Technol. **80**, 168–173 (2016)
22. H. Gencer, M. Pektas, Y. Babur, V.S. Kolat, T. Izgi, S. Atalay, Electrical transport and magnetoresistance of $La_{0.67}Ca_{0.33}MnO_3$:Ag_x (x = 0, 0.1, 0.2, 0.3, 0.4) composites. Jpn. Magn. **17**(3), 176–184 (2012)
23. F. Mikailzade, F. Onal, M. Maksutoglu, M. Zarbali, Structure and magnetization of polycrystalline $La_{0.66}Ca_{0.33}MnO_3$ and $La_{0.66}Ba_{0.33}MnO_3$ films prepared using sol-gel technique. J. Supercond. Nov. Magn. **31**, 4141–4145 (2018)
24. H. Gencer, A. Goktas, M. Gunes, H.I. Mutlu, S. Atalay, H. Kishan, Enhanced room temperature coeffificient of resistance and magnetoresistance of Ag-added La0.7Ca0.3-xBaxMnO3 composites. J. Phys. D Appl. Phys. **42**(17), 175002–175008 (2009)
25. K. Daoudi, T. Tsuchiya, T. Kumagai, Growth and characterization of epitaxial magnetoresistance properties of $La_{0.67}Ca_{0.33}MnO_3$ film coated on pyrex glass substrate. Int. J. Mod. Phys. **22**, 497–506 (2008)
26. N. Kumar, H. Kishan, A. Rao, V.P.S. Awana, Fe ion doping effect on electrical and magnetic properties of $La_{0.7}Ca_{0.3}Mn_{1-x}Fe_xO_3$ ($0 \le x \le 1$). J. Alloys Compd. **502**, 283–288 (2010)

27. S. Zhao, X. Yue, X. Liu, Tuning room temperature Tp and MR of $La_{1-y}(Ca_{y-x}Sr_x)MnO_3$ polycrystalline ceramics by Sr doping. Ceram. Int. **43**, 4594–4598 (2017)
28. T. Sudyoadsuk, R. Suryanarayanan, P. Winotai, Effect of Cr and Fe substitutions on the magnetotransport properties of the charge-ordered manganite $La_{0.4}Ca_{0.6}MnO_3$. J. Magn. Magn. Mater. **272**, 1379–1382 (2004)